


# Charge self-consistent dynamical mean field theory calculations in combination with linear combination of numerical atomic orbitals framework based density functional theory

Xin Qu(瞿鑫), Peng Xu(许鹏), Zhiyong Liu(刘志勇), Jintao Wang(王金涛), Fei Wang(王飞), Wei Huang(黄威), Zhongxin Li(李忠星), Weichang Xu(徐卫昌), and Xinguo Ren(任新国)

**Citation:**Chin. Phys. B, 2024, 33 (**10**): 107106. DOI: 10.1088/1674-1056/ad6558
Journal homepage: http://cpb.iphy.ac.cn; http://iopscience.iop.org/cpb

**What follows is a list of articles you may be interested in**

---

## Optimized numerical density functional theory calculation of rotationally symmetric jellium model systems

Guangdi Zhang(张广迪), Li Mao(毛力), and Hongxing Xu(徐红星)
Chin. Phys. B, 2024, 33 (**10**): 107101. DOI: 10.1088/1674-1056/ad655a

## Half-metallic ferromagnetic Weyl fermions related to dynamic correlations in the zinc-blende compound VAs

Xianyong Ding(丁献勇), Haoran Wei(魏皓然), Ruixiang Zhu(朱瑞翔), Xiaoliang Xiao(肖晓亮), Xiaozhi Wu(吴小志), and Rui Wang(王锐)
Chin. Phys. B, 2024, 33 (**9**): 097103. DOI: 10.1088/1674-1056/ad5f86

## Coexistence of Dirac and Weyl points in non-centrosymmetric semimetal $NbIrTe_4$

Qingxin Liu(刘清馨), Yang Fu(付阳), Pengfei Ding(丁鹏飞), Huan Ma(马欢), Pengjie Guo(郭朋杰), Hechang Lei(雷和畅), and Shancai Wang(王善才)
Chin. Phys. B, 2024, 33 (**4**): 047104. DOI: 10.1088/1674-1056/ad2a79

## Angle-resolved photoemission study of NbGeSb with non-symmorphic symmetry

Huan Ma(马欢), Ning Tan(谭宁), Xuchuan Wu(吴徐传), Man Li(李满), Yiyan Wang(王义炎), Hongyan Lu(路洪艳), Tianlong Xia(夏天龙), and Shancai Wang(王善才)
Chin. Phys. B, 2024, 33 (**2**): 027102. DOI: 10.1088/1674-1056/ad0ccf

## Implementation of LDA+DMFT with the pseudo-potential-plane-wave method

Zhao Jian-Zhou(赵建洲), Zhuang Jia-Ning(庄嘉宁), Deng Xiao-Yu(邓小宇), Bi Yan(毕延), Cai Ling-Cang(蔡灵仓), Fang Zhong(方忠), and Dai Xi(戴希)
Chin. Phys. B, 2012, 21 (**5**): 057106. DOI: 10.1088/1674-1056/21/5/057106

---

**COMPUTATIONAL PROGRAMS FOR PHYSICS**

# Charge self-consistent dynamical mean field theory calculations in combination with linear combination of numerical atomic orbitals framework based density functional theory

Xin Qu(瞿鑫)[1], Peng Xu(许鹏)[2,†], Zhiyong Liu(刘志勇)[3], Jintao Wang(王金涛)[2], Fei Wang(王飞)[2], Wei Huang(黄威)[1], Zhongxin Li(李忠星)[1], Weichang Xu(徐卫昌)[1], and Xinguo Ren(任新国)[4,‡]

[1] *Qingzhou High Technology Institute, Weifang* 262500, *China*
[2] *Rocket Force University of Engineering, Xi'an* 710025, *China*
[3] *Beijing Research Institute of High Technology, Beijing* 100077, *China*
[4] *Institute of Physics, Chinese Academy of Sciences, Beijing* 100190, *China*

(Received 29 May 2024; revised manuscript received 10 July 2024; accepted manuscript online 19 July 2024)

We present a formalism of charge self-consistent dynamical mean field theory (DMFT) in combination with density functional theory (DFT) within the linear combination of numerical atomic orbitals (LCNAO) framework. We implemented the charge self-consistent DFT + DMFT formalism by interfacing a full-potential all-electron DFT code with three hybridization expansion-based continuous-time quantum Monte Carlo impurity solvers. The benchmarks on several 3d, 4f and 5f strongly correlated electron systems validated our formalism and implementation. Furthermore, within the LCANO framework, our formalism is general and the code architecture is extensible, so it can work as a bridge merging different LCNAO DFT packages and impurity solvers to do charge self-consistent DFT + DMFT calculations.

**Keywords:** dynamical mean field theory, density functional theory, strongly correlated electrons

**PACS:** 71.15.Mb, 71.15.–m **DOI:** 10.1088/1674-1056/ad6558

## 1. Introduction

The failure of traditional Kohn–Sham (KS) density functional theory (DFT) to quantitatively or even qualitatively correctly describe a large series of strongly correlated materials[1–4] calls for more advanced methods beyond conventional LDA/GGA.[1,2,5–14] Among these methods, the DFT + DMFT that combines the DFT and dynamical mean field theory (DMFT) using non-perturbative technique within many-body language, has been accepted as a powerful and promising many-body method to tackle this problem, due to its remarkable success in describing the electronic structures of strongly correlated materials.[3,4,15–18]

To our knowledge, there are two types of DFT + DMFT schemes till now. The first scheme does not invoke corrections for the non-interacting KS charge density by incorporating the influence of the DMFT self-energy on the charge density. This type of DFT + DMFT scheme is termed as non-charge-self-consistent DFT + DMFT or more usually as the one-shot DFT + DMFT. The second scheme runs self-consistency on a higher level, which includes not only the self-consistency over the self-energy but also over the charge density. This kind of DFT + DMFT scheme generally consists of four steps: Firstly, perform a DFT calculation to get well-converged results with high quality. Secondly, starting from the DFT results, run DMFT calculations to get the dynamical self-energy. Thirdly, update the charge density using the DMFT self-energy. Fourthly, carry out a one-step DFT calculation with the updated charge density, and then return to the second step. The self-consistent cycle will continue until both the self-energy and charge density achieve convergence.

In the past few decades, many charge self-consistent DFT + DMFT implementations were developed within different basis set frameworks. The first charge self-consistent DFT + DMFT scheme was developed by Savrasov and Kotliar within the linear muffin-tin orbital (LMTO) basis set.[19] With the plane wave (PW) method, the charge self-consistent DFT + DMFT implementations within Quantum ESPRESSO (QE)[20,21] and CASTEP[22] have been reported. In the QE-based implementation, the Wannier orbitals constructed by Wannier90[23–26] were used to define local correlated orbitals. As for the projector augmented wave (PAW) framework, charge self-consistent DFT + DMFT were implemented in combination with two popular softwares, i.e., the VASP[27] and the ABINIT.[28,29] Last but not least, the charge self-consistent DFT + DMFT method has also been implemented within the full-potential all-electron linearized augmented plane-wave (LAPW) framework, in particular within the WIEN2k[30,31] and ELK.[32] Among these charge self-

†Corresponding author. E-mail: xupeng76345@163.com
‡Corresponding author. E-mail: renxg@iphy.ac.cn

© 2024 Chinese Physical Society and IOP Publishing Ltd 

consistent DFT + DMFT implementations within yjr LAPW framework, the eDMFT[30] developed by Haule *et al.* in combination with WIEN2k has the most abundant features.

In recent years, the linear combination of numerical atomic orbitals (LCNAO) has become a versatile framework for implementing various kinds of conventional and advanced methods of modern DFT.[33–36] Up to date, only a few DFT + DMFT schemes within the framework of LCNAO have been reported. The first one-shot DFT + DMFT implementation within LCNAO framework was reported by Sim and Han[37] in combination with OpenMX. Recently, we developed the second LCNAO-based one-shot DFT + DMFT using rather different techniques.[38] However, to our knowledge, there is no charge self-consistent DFT + DMFT implementation within the framework of LCNAO basis set. This work aims to develop a charge self-consistent DFT + DMFT formalism and implementation within the framework of LCNAO based on our previous one-shot work.[38]

This paper is structured as follows. Section 2 presents the charge self-consistent DFT + DMFT formalism within the LCNAO framework. On the basis of our one-shot DFT + DMFT formalism, we update the KS non-interacting charge density through embedding the self-energy back to the full Hilbert space, and then construct a charge self-consistent DFT + DMFT formalism that loops over both self-energy and charge density. Section 3 presents the computational details. In Section 4, we carry out calculations on several typical strongly correlated systems to benchmark our charge self-consistent DFT + DMFT formalism and implementation, including 3d electron systems $SrVO_3$ and NiO, 4f lanthanides systems $\alpha$- and $\gamma$-Ce, and 5f actinide system $UO_2$. Finally, Section 5 concludes the paper.

## 2. Formalism

### 2.1. Charge density updating

The charge self-consistent DFT + DMFT algorithm in this paper is based on our recently developed one-shot DFT + DMFT scheme.[38] The key issue to implement the charge self-consistent DFT + DMFT algorithm is to update the charge density by incorporating the effect of the self-energy, which includes the complex many-body correlation among the strongly correlated electrons. In terms of the Green's function, the charge density in real space can be written as

$$\begin{aligned}\rho(\boldsymbol{r}) &= G\left(\boldsymbol{r},\boldsymbol{r}';0^-\right)|_{\boldsymbol{r}=\boldsymbol{r}'}\\ &= -G\left(\boldsymbol{r},\boldsymbol{r}';\beta^-\right)|_{\boldsymbol{r}=\boldsymbol{r}'}\\ &= -\frac{1}{\beta}\sum_n G\left(\boldsymbol{r},\boldsymbol{r}';\mathrm{i}\omega_n\right)\mathrm{e}^{-\mathrm{i}\omega_n\beta^-}|_{\boldsymbol{r}=\boldsymbol{r}'},\end{aligned}\tag{1}$$

where $G$ is the Green's function, with $\beta = 1/(k_{\mathrm{B}}T)$ the inverse temperature and the $\omega_n = (2n+1)\pi/\beta$ the Matsubara frequency. Within the KS basis representation, Eq. (1) becomes

$$\begin{aligned}\rho(\boldsymbol{r}) = &-\frac{1}{\beta}\sum_{\boldsymbol{k}}\sum_{ij}\sum_n \Psi_{i\boldsymbol{k}}(\boldsymbol{r})\\ &\times\left[\frac{1}{(\mathrm{i}\omega_n+\mu-\epsilon_{\boldsymbol{k}})I-\bar{\Sigma}(\boldsymbol{k},\mathrm{i}\omega_n)}\right]_{ij}\\ &\times\Psi^*_{j\boldsymbol{k}}(\boldsymbol{r})\,\mathrm{e}^{-\mathrm{i}\omega_n\beta^-},\end{aligned}\tag{2}$$

where $\mu$ is the chemical potential, $\epsilon_{\boldsymbol{k}}$ the diagonal matrix containing the KS eigenvalues, and $\Psi_{i\boldsymbol{k}}(\boldsymbol{r})$ the KS eigenfunctions. Here, $I$ is the identity matrix, $i$ and $j$ denote the band index, and $\boldsymbol{k}$ is the sampling point in the first Brillouin zone. $\bar{\Sigma}$ is the self-energy in the full KS space, which is embedded back from the strongly correlated subspace. In analogy with our previous work,[38] the DMFT calculations are conducted in a correlated subset of bands around the Fermi level (denoted as $\mathcal{C}$), and therefore the self-energy $\bar{\Sigma}(\boldsymbol{k},\mathrm{i}\omega_n)$ is non-zero unless both bands $i$ and $j$ belong to the correlated subset $\mathcal{C}$. Given this property of the self-energy, the charge density $\rho(\boldsymbol{r})$ can be decomposed into two parts, i.e.,

$$\begin{aligned}\rho(\boldsymbol{r}) &= \rho_{\mathrm{c}}(\boldsymbol{r})+\rho_{\mathrm{uc}}(\boldsymbol{r})\\ &= -\frac{1}{\beta}\sum_{\boldsymbol{k}}\sum_{i,j\in\mathcal{C}}\sum_n \Psi_{i\boldsymbol{k}}(\boldsymbol{r})\\ &\quad\times\left[\frac{1}{(\mathrm{i}\omega_n+\mu-\epsilon_{\boldsymbol{k}})I-\bar{\Sigma}(\boldsymbol{k},\mathrm{i}\omega_n)}\right]_{ij}\\ &\quad\times\Psi^*_{j\boldsymbol{k}}(\boldsymbol{r})\,\mathrm{e}^{-\mathrm{i}\omega_n\beta^-}\\ &\quad-\frac{1}{\beta}\sum_{\boldsymbol{k}}\sum_{i\notin\mathcal{C}}\sum_n \Psi_{i\boldsymbol{k}}(\boldsymbol{r})\left[\frac{1}{(\mathrm{i}\omega_n+\mu-\epsilon_{\boldsymbol{k}})I}\right]_{ii}\\ &\quad\times\Psi^*_{i\boldsymbol{k}}(\boldsymbol{r})\,\mathrm{e}^{-\mathrm{i}\omega_n\beta^-}\\ &= -\frac{1}{\beta}\sum_{\boldsymbol{k}}\sum_{i,j\in\mathcal{C}}\sum_n \Psi_{i\boldsymbol{k}}(\boldsymbol{r})G^{\mathrm{int}}_{ij}(\boldsymbol{k},\mathrm{i}\omega_n)\Psi^*_{j\boldsymbol{k}}(\boldsymbol{r})\,\mathrm{e}^{-\mathrm{i}\omega_n\beta^-}\\ &\quad-\frac{1}{\beta}\sum_{\boldsymbol{k}}\sum_{i\notin\mathcal{C}}\sum_n \Psi_{i\boldsymbol{k}}(\boldsymbol{r})G^{\mathrm{KS}}_{ii}(\boldsymbol{k},\mathrm{i}\omega_n)\Psi^*_{i\boldsymbol{k}}(\boldsymbol{r})\,\mathrm{e}^{-\mathrm{i}\omega_n\beta^-}\\ &= \sum_{\boldsymbol{k}}\sum_{i,j\in\mathcal{C}}\Psi_{i\boldsymbol{k}}(\boldsymbol{r})N^{\mathrm{c}}_{ij}(\boldsymbol{k})\Psi^*_{j\boldsymbol{k}}(\boldsymbol{r})\\ &\quad+\sum_{\boldsymbol{k}}\sum_{i\notin\mathcal{C}}\Psi_{i\boldsymbol{k}}(\boldsymbol{r})N^{\mathrm{uc}}_{ii}(\boldsymbol{k})\Psi^*_{i\boldsymbol{k}}(\boldsymbol{r}).\end{aligned}\tag{3}$$

The $\rho_{\mathrm{uc}}(\boldsymbol{r})$ is the uncorrelated part consisting of the non-interacting electrons outside the subset $\mathcal{C}$ while the $\rho_{\mathrm{c}}(\boldsymbol{r})$ the correlated part consisting of the interacting electrons within the subset $\mathcal{C}$. In Eq. (3), the interacting and non-interacting Green's functions respectively are

$$G^{\mathrm{int}}_{ij}(\boldsymbol{k},\mathrm{i}\omega_n) = \left[\frac{1}{(\mathrm{i}\omega_n+\mu-\epsilon_{\boldsymbol{k}})I-\bar{\Sigma}(\boldsymbol{k},\mathrm{i}\omega_n)}\right]_{ij},\tag{4}$$

$$G^{\mathrm{KS}}_{ii}(\boldsymbol{k},\mathrm{i}\omega_n) = \left[\frac{1}{(\mathrm{i}\omega_n+\mu-\epsilon_{\boldsymbol{k}})I}\right]_{ii}.\tag{5}$$

Consequently, the interacting and non-interacting occupation matrices

$$N^{\mathrm{c}}_{ij}(\boldsymbol{k}) = -\frac{1}{\beta}\sum_n G^{\mathrm{int}}_{ij}(\boldsymbol{k}, \mathrm{i}\omega_n)\mathrm{e}^{-\mathrm{i}\omega_n\beta^-}, \tag{6}$$

$$N^{\mathrm{uc}}_{ii}(\boldsymbol{k}) = -\frac{1}{\beta}\sum_n G^{\mathrm{KS}}_{ii}(\boldsymbol{k}, \mathrm{i}\omega_n)\mathrm{e}^{-\mathrm{i}\omega_n\beta^-} \tag{7}$$

are given by summation of the Green's functions over the Matsubara frequencies.

Since the non-interacting KS Green's function $G^{\mathrm{KS}}$ in Eq. (5) is diagonal, the summation over the Matsubara frequencies in Eq. (7) from minus infinity to positive infinity yields the KS band occupation number $f_{i\boldsymbol{k}}$, i.e.,

$$N^{\mathrm{uc}}_{ii}(\boldsymbol{k}) = f_{i\boldsymbol{k}} = \frac{1}{1+\mathrm{e}^{\beta(\epsilon_{i\boldsymbol{k}}-\mu)}}. \tag{8}$$

The presence of non-diagonal elements in interacting Green's function $G^{\mathrm{int}}$ arising from the self-energy $\bar{\Sigma}$ renders that the trick employed in Eq. (8) fails on the summation over Matsubara frequencies in Eq. (6). To deal with this complexity, we divide $G^{\mathrm{int}}$ into two parts, i.e.,

$$G^{\mathrm{int}}_{ij}(\boldsymbol{k}, \mathrm{i}\omega_n) = \begin{cases} \left[\frac{1}{(\mathrm{i}\omega_n+\mu-\epsilon_{\boldsymbol{k}})I-\bar{\Sigma}(\boldsymbol{k},\mathrm{i}\omega_n)}\right]_{ij}, & n \le N, \\ \left[\frac{1}{(\mathrm{i}\omega_n+\mu-\epsilon_{\boldsymbol{k}})I-\bar{\Sigma}(\boldsymbol{k},\mathrm{i}\omega_\infty)}\right]_{ij}, & n > N, \end{cases} \tag{9}$$

where $N$ specifies certain cutoff frequency $\omega_N$. For the first part below the cut-off frequency $\omega_N$, its summation is numerically calculated directly. As for the second part above the cut-off frequency, the self-energy is approximated by its high frequency limit $\bar{\Sigma}_{ij}(\boldsymbol{k}, \mathrm{i}\omega_\infty)$, which is Hermitian. Therefore, Eq. (6) becomes

$$\begin{aligned} N^{\mathrm{c}}_{ij}(\boldsymbol{k}) = & \frac{1}{\beta}\sum_{\omega_n=-\omega_N}^{\omega_N}\left(\left[\frac{1}{(\mathrm{i}\omega_n+\mu-\epsilon_{\boldsymbol{k}})I-\bar{\Sigma}(\boldsymbol{k},\mathrm{i}\omega_n)}\right]_{ij}\right. \\ & \left.-\left[\frac{1}{(\mathrm{i}\omega_n+\mu-\epsilon_{\boldsymbol{k}})I-\bar{\Sigma}(\boldsymbol{k},\mathrm{i}\omega_\infty)}\right]_{ij}\right) \\ & +\frac{1}{\beta}\sum_{\omega_n}\left[\frac{1}{(\mathrm{i}\omega_n+\mu-\epsilon_{\boldsymbol{k}})I-\bar{\Sigma}_{ij}(\boldsymbol{k},\mathrm{i}\omega_\infty)}\right]_{ij}. \end{aligned} \tag{10}$$

As mentioned above, the first summation in Eq. (10) on the right-hand side is directly computed, and the result is denoted as $n^{\mathrm{nu}}_{ij}(\boldsymbol{k})$. The second summation in Eq. (10) is coped with the following two steps. Firstly, make a representation transform from the original KS basis to the basis consisting of eigen-wavefunctions of the Hermitian Hamiltonian $H_{ij}(\boldsymbol{k}, \mathrm{i}\omega_\infty) = \epsilon_{i\boldsymbol{k}}\delta_{ij} + \bar{\Sigma}_{ij}(\boldsymbol{k}, \mathrm{i}\omega_\infty)$. The eigenfunctions of this Hamiltonian are obtained as

$$\sum_j H_{ij}(\boldsymbol{k}, \mathrm{i}\omega_\infty)\tilde{c}_{\lambda,j}(\boldsymbol{k}, \mathrm{i}\omega_\infty) = \epsilon^{\mathrm{eff}}_\lambda(\boldsymbol{k}, \mathrm{i}\omega_\infty)\tilde{c}_{\lambda,i}(\boldsymbol{k}, \mathrm{i}\omega_\infty), \tag{11}$$

where $\epsilon^{\mathrm{eff}}_\lambda(\boldsymbol{k}, \mathrm{i}\omega_\infty)$ is the $\lambda$-th eigenvalue, $\tilde{c}_{\lambda,i}(\boldsymbol{k}, \mathrm{i}\omega_\infty)$ the coefficients of the eigenfunction. Within this basis, the Green's function becomes diagonal, i.e.,

$$G_{\lambda\lambda'}(\boldsymbol{k}, \mathrm{i}\omega_\infty) = \left[\frac{1}{\mathrm{i}\omega_n+\mu-\epsilon^{\mathrm{eff}}(\boldsymbol{k}, \mathrm{i}\omega_\infty)}\right]_{\lambda\lambda'}\delta_{\lambda\lambda'}. \tag{12}$$

Taking advantage of the same trick used in Eq. (8), the summation yields

$$\frac{1}{1+\mathrm{e}^{\beta(\epsilon^{\mathrm{eff}}_\lambda(\boldsymbol{k},\mathrm{i}\omega_\infty)-\mu)}}.$$

Secondly, carrying out an inverse transform of the representation to get the second summation in Eq. (10) as

$$\begin{aligned} n^{\mathrm{lim}}_{ij}(\boldsymbol{k}) = & \sum_\lambda \tilde{c}_{\lambda,i}(\boldsymbol{k}, \mathrm{i}\omega_\infty)\frac{1}{1+\mathrm{e}^{\beta(\epsilon^{\mathrm{eff}}_\lambda(\boldsymbol{k},\mathrm{i}\omega_\infty)-\mu)}} \\ & \times\tilde{c}^*_{\lambda,j}(\boldsymbol{k}, \mathrm{i}\omega_\infty). \end{aligned} \tag{13}$$

Finally, the charge density in Eq. (3) can be calculated as

$$\rho(\boldsymbol{r}) = \sum_{\boldsymbol{k}}\sum_{i,j\in\mathcal{C}}\Psi_{i\boldsymbol{k}}(\boldsymbol{r})n_{ij}(\boldsymbol{k})\Psi^*_{j\boldsymbol{k}}(\boldsymbol{r}), \tag{14}$$

wherein

$$n_{ij}(\boldsymbol{k}) = \begin{cases} f_{i\boldsymbol{k}}\delta_{ij}, & i\notin\mathcal{C} \text{ or } j\notin\mathcal{C}, \\ n^{\mathrm{nu}}_{ij}(\boldsymbol{k}) + n^{\mathrm{lim}}_{ij}(\boldsymbol{k}), & i\in\mathcal{C} \text{ and } j\in\mathcal{C}. \end{cases} \tag{15}$$

In the implementation, the density matrix

$$\rho_{\mu\nu}(\boldsymbol{k}) = \frac{1}{N_{\boldsymbol{k}}}\sum_{ij} n_{ij}(\boldsymbol{k})c_{i\boldsymbol{k},\mu}c^*_{j\boldsymbol{k},\nu} \tag{16}$$

rather than the charge density $\rho(\boldsymbol{r})$ in real space is used. In Eq. (16), $N_{\boldsymbol{k}}$ is the number of sampling points in the first Brillouin zone, $c_{i\boldsymbol{k},\mu}$ and $c_{j\boldsymbol{k},\nu}$ the KS eigencoefficients within the NAO basis set. This choice has three advantages compared to dealing directly with the real-space charge density. Firstly, different NAO schemes usually employ rather different real-space grid techniques, which leads to lots of additional works on constructing the real-space charge density via Eq. (14) if one intends to interface our implementation with different NAO-based DFT codes. Secondly, within the NAO scheme, the density matrix not only uniquely determines the charge density but also contains additional useful information. For example, the density matrix could provide adequate and necessary information for hybrid functional calculations, which is otherwise not possible with only the real-space charge density. Thirdly, since the density matrix does not include basis orbitals, the calculation of density matrix will be much simpler than calculating the charge density on the real-space grid.

### 2.2. Implementation

As shown in Fig. 1, charge self-consistent DFT + DMFT calculations in our implementation are done in the following major steps.

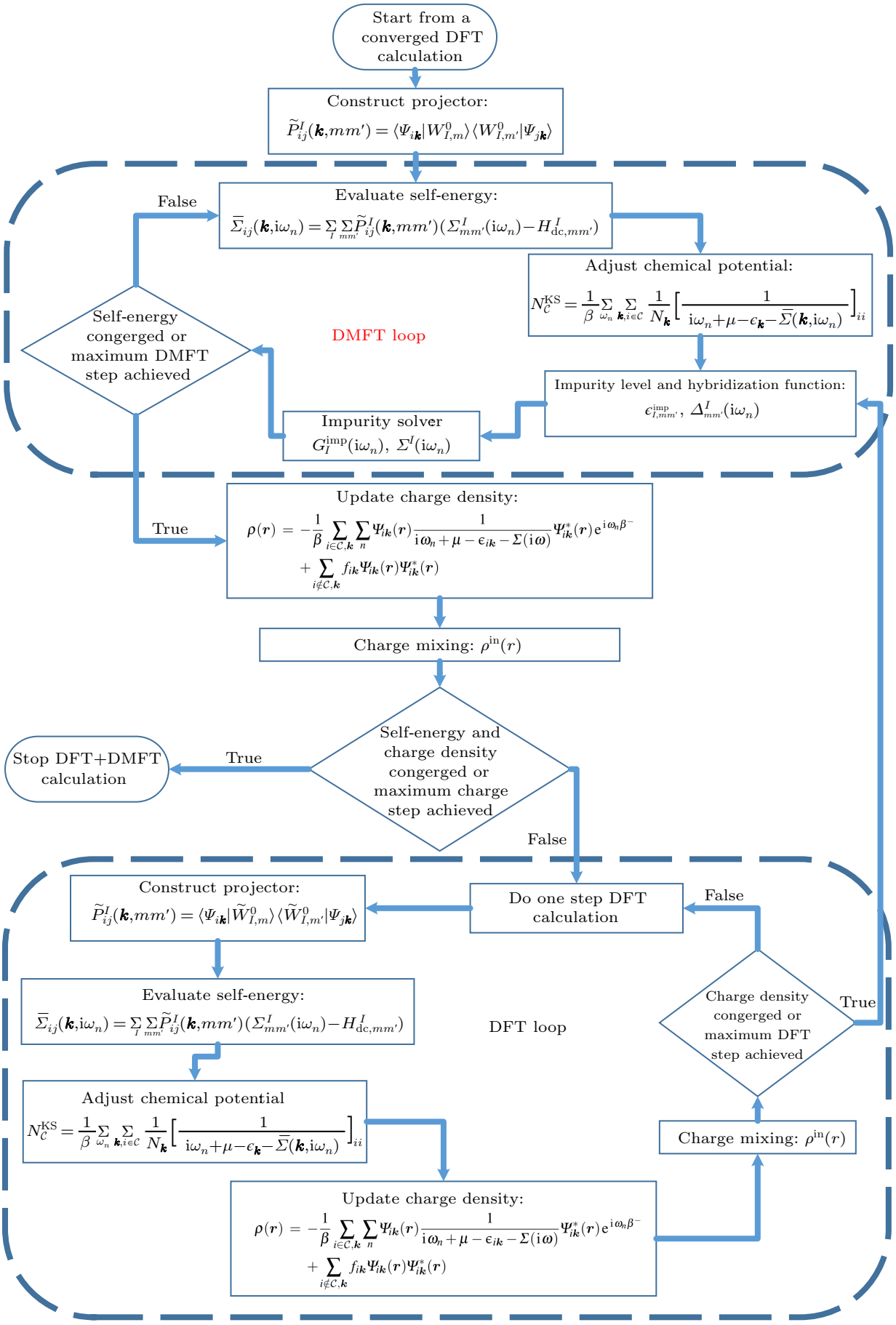



**Fig. 1.** Flow diagram of our charge self-consistent DFT + DMFT implementation.

**Step 1** Carry out a high-quality self-consistent DFT calculation.

**Step 2** Construct the projector within the formalism detailedly introduced in Subsection 2.2 of our recent one-shot DFT + DMFT paper.[38]

**Step 3** Update the self-energy $\bar{\Sigma}_{ij}(\boldsymbol{k}, \mathrm{i}\omega_n)$. Using Eq. (25) in our one-shot DFT + DMFT paper,[38] we embed the latest impurity self-energy back to the selected KS space subset $\mathcal{C}$ to get $\bar{\Sigma}_{ij}(\boldsymbol{k}, \mathrm{i}\omega_n)$ within the projector constructed in step 2. Except for the first step, where the double-counting term is guessed as the initial self-energy, the self-energy of the current step is given by the impurity solver in the last step.

**Step 4** Adjust chemical potential $\mu$. Since the self-energy has been updated in the last step, to keep the number of electrons contained by KS bands in $\mathcal{C}$ subset conserved, the chemical potential needs to be adjusted accordingly.

**Step 5** Calculate the impurity level and the hybridization function using Eqs. (29)–(31) in our recent one-shot DFT + DMFT paper.[38]

**Step 6** Solve the mapped Anderson impurity problem. Pass the updated chemical potential, impurity level, hybridization function and the on-site Coulomb interaction parameters to the impurity solver and then the new impurity self-energy and Green's function are obtained.

**Step 7** Check whether the self-energy converges or the maximum DMFT step is reached. If both of the two criteria are not met, go back to step 4; otherwise stop the so-called DMFT loop, which drops steps 3–6.

**Step 8** Charge density updating. Update the charge density with the latest self-energy via the method introduced in Subsection 2.1.

**Step 9** Charge density mixing. The previous experience tells us that calculations usually diverge without charge density mixing, and so it is of great importance to mix the updated charge density with those of the latest few steps. In our implementation, the Pulay DIIS (direct inversion of the iterative subspace, DIIS)[39,40] method is employed to mix the charge densities. After finishing the charge density mixing, check whether both the charge density and the self-energy converge or not. If the convergence criteria are satisfied, stop the whole charge self-consistent DFT + DMFT calculation; otherwise go to the next step.

**Step 10** Do a one-step non-self-consistent LDA/GGA calculation to get new KS wave function and band structures.

**Step 11** Construct the projector based on the non-self-consistent LDA/GGA results of the last step.

**Step 12** Embed the DMFT self-energy in the local correlated subspace back to the KS space as step 3.

**Step 13** Adjust the chemical potential using the latest self-energy and non-self-consistent LDA/GGA results.

**Step 14** Update charge density as step 8.

**Step 15** Mix charge density as step 9.

**Step 16** Check the charge density convergence. If the charge density converges or the DFT loop reaches the maximum step, go to step 5; otherwise go back to step 10. The so-called DFT loop groups steps 10–16 together. The whole loop from step 3 to 16 including the DMFT and DFT loop comprises one full charge loop.

## 3. Computational details

In this paper, we carried out charge self-consistent DFT + DMFT calculations on four prototypical strongly correlated materials, i.e., two d systems and two f systems, to benchmark our formalism and implementation. All DFT calculations were carried out by using the full-potential all-electron LCNAO package FHI-aims.[35] In FHI-aims, the default *tight tier 1* basis set was adopted for all elements. As for the exchange–correlation functional, the Perdew–Burke–Ernzerhof (PBE) GGA functional was employed.[41] Three CT-HYB (hybridization expansion-based continuous-time quantum Monte Carlo) impurity solvers,[42] i.e., PACS,[43] iQIST,[44–46] and Rutgers eDMFT[47,48] as denoted in Ref. [38], were used for solving the single-site Anderson impurity model in the DMFT part.

The band structure, i.e., $\epsilon_{i\boldsymbol{k}}$, was not invariant during the self-consistent iteration, which would cause instability for determining the correlated subset $\mathcal{C}$ if the energy window was fixed. To solve this problem, we fixed the lower and upper limits of the bands as the ones used in the first DMFT step within the first charge loop, and the correlated subset $\mathcal{C}$ was composed of the full bands with indices within the window defined by the lower and upper limits.

## 4. Results and discussion

### 4.1. The 3d electron systems

The first two benchmarks of our charge self-consistent DFT + DMFT algorithm and implementation were carried out on two typical strongly correlated 3d systems, i.e., $SrVO_3$ and NiO.

#### 4.1.1. $SrVO_3$

In the DFT part, we used the Monkhorst–Pack method[49] to sample the Brillouin zone with a $\Gamma$ centered $11 \times 11 \times 11$ $\boldsymbol{k}$-mesh. As for the DMFT part, the $U$ and $J$ were chosen as 4.0 eV and 0.65 eV, respectively, following Refs. [37,50,51]. The temperature was 300 K. The correlated subset $\mathcal{C}$ was composed of six bands crossing the Fermi level with band indices (in an all-electron calculation) running from 41 to 46. In the case of $V^{4+}$, the two $e_g$ orbitals with higher energy are empty, we considered only three degenerate $t_{2g}$ orbitals with lower energy in our charge self-consistent DFT + DMFT calculations.

These parameters are the same as the ones used in our previous one-shot DFT + DMFT calculations.[38]

As shown in Fig. 2, the spectral functions of $SrVO_3$ 3d electrons obtained by charge self-consistent and one-shot DFT + DMFT calculations are nearly identical with minor differences. It indicates that the charge self-consistent DFT + DMFT results are in good agreement with previous theoretical results[37,50–56] and experiments[57] as discussed in our one-shot DFT + DMFT work.[38] Additionally, the minor difference between the charge self-consistent and one-shot DFT + DMFT suggests that the charge density updating using DMFT self-energy has a negligible influence on the electron spectral functions.

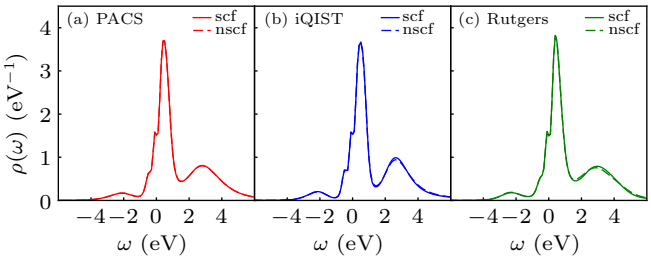



**Fig. 2.** The charge self-consistent and one-shot DFT + DMFT spectral functions of $SrVO_3$ 3d electrons. The results were given by three CT-HYB impurity solvers, PACS (a), iQIST (b) and Rutgers (c). The solid lines labeled with "scf" are results of charge self-consistent DFT + DMFT calculations, while the dashed lines labeled with "nscf" the results of one-shot DFT + DMFT calculations taken from Ref. [38].

#### 4.1.2. NiO

In DFT calculations, the $\Gamma$-centered $11 \times 11 \times 11$ $\boldsymbol{k}$-grid was generated by the Monkhorst–Pack method[49] for the sampling of the first Brillouin zone. The DMFT calculations were performed with $U = 8.0$ eV and $J = 1.0$ eV at $T = 1160$ eV, consistent with the choices used in the literature.[1,37,58,59] The subset of KS bands $\mathcal{C}$ encloses all those overlapping with the energy window $[-2.0\,\text{eV}, 1.0\,\text{eV}]$. All parameters are the same as those used in our recent one-shot DFT + DMFT work.[38]

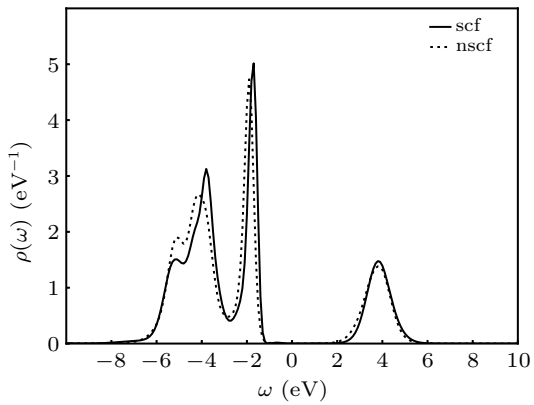



**Fig. 3.** The charge self-consistent and one-shot DFT + DMFT spectral functions of NiO 3d electrons. The solid black line labeled with "scf" is the result of charge self-consistent DFT + DMFT, while the dotted black line labeled with "nscf" is the result of one-shot DFT + DMFT obtained from our recent work.[38]

Figure 3 shows the 3d electrons spectra of NiO obtained by charge self-consistent and one-shot DFT + DMFT calculations. The main features of two spectra, e.g., the shape, intensity and the location of the peaks are very similar. It suggests that the charge self-consistent DFT + DMFT results are in good agreement with both previous theoretical and experimental results.[58–60] In comparison to $SrVO_3$, the difference between the charge self-consistent and one-shot DFT + DMFT of NiO is more distinct. This may indicate that the correlation of 3d electrons in NiO is stronger than that in $SrVO_3$.

### 4.2. The 4f electron systems

Next we benchmark our charge self-consistent DFT + DMFT formalism and implementation on 4f lanthanides, i.e., the $\gamma \rightarrow \alpha$ phase transition of the cerium metal. In the DFT parts, $\Gamma$-centered $11 \times 11 \times 11$ Monkhorst–Back $\boldsymbol{k}$-point mesh was used for the Brillouin zone integration. The crystal structures of $\alpha$- and $\gamma$-Ce phases in the transition were modeled by FCC cells with different volumes, i.e., 29 Å$^3$ for $\alpha$ and 34 Å$^3$ for $\gamma$ phase.[61] All DMFT calculations were done by the Rutgers impurity solver at the temperature of 800 K[62] with parameters of $U = 6.0$ eV and $J = 0.5$ eV.[62,63] The KS subset $\mathcal{C}$ was determined by the energy window $[-5.0\,\text{eV}, 5.0\,\text{eV}]$. All parameters are the same as those used in our one-shot work[38] to facilitate a direct comparison.

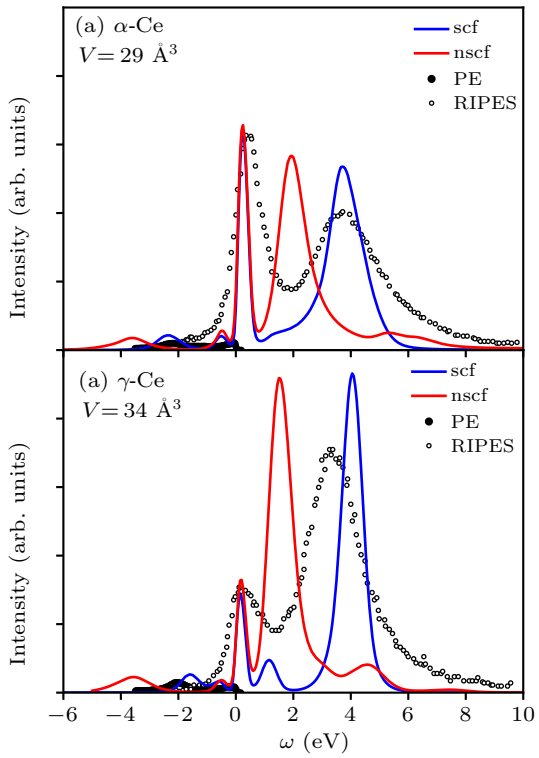



**Fig. 4.** The theoretical and experimental 4f-spectra of $\alpha$- and $\gamma$-Ce. The blue solid lines labeled with "scf" are the results obtained by charge self-consistent DFT + DMFT calculations, while the red solid lines labeled with "nscf" are the one-shot DFT + DMFT results taken from our previous work.[38] The experimental results, i.e., the RIPES (resonant inverse photoemission spectroscopy) and PE (photoemission) came from Refs. [64,65].

Figure 4 shows the experimental (resonant inverse photoemission and photoemission) and theoretical (one-shot and charge self-consistent DFT + DMFT) 4f-electron spectra of $\alpha$- and $\gamma$-Ce. As is clearly shown, the introduction of self-consistency on the charge density prominently improves the quality of results, compared to the one-shot DFT + DMFT calculations. This improvement is mainly reflected in two aspects. Firstly, the locations of the upper Hubbard bands of 4f electrons of $\alpha$- and $\gamma$-Ce predicted by the charge self-consistent DFT + DMFT calculations agree well with experiments, whereas approximately 2.0 eV deviation exists in the results of the one-shot DFT + DMFT calculations. Secondly, the charge self-consistent DFT + DMFT calculations successfully reproduce the lower Hubbard band at around $-2.0$ eV, while the one-shot DFT + DMFT fails to do so. Generally, the results given by charge self-consistent DFT + DMFT agree much better with experiments than one-shot DFT + DMFT both qualitatively and quantitatively. This result reveals the importance of self-consistency over the charge density on the $\alpha$- and $\gamma$-Ce due to the strong many-body correlation of the 4f electrons. In comparison to previous theoretical results, our charge self-consistent DFT + DMFT spectra of 4f electrons of $\alpha$- and $\gamma$-Ce are in good agreement with the charge self-consistent DFT + DMFT results reported by Bieder *et al.*[62]

### 4.3. The 5f electron system

In this section, we benchmark our implementation on a prototypical actinide system, $UO_2$. $UO_2$ is an important nuclear fuel. As an actinide oxide, it exhibits many exotic phenomena arising from the strong correlation among electrons in the open 5f shell, where the failures of traditional LDA/GGA functionals have been clearly demonstrated.[66] Therefore, an accurate description of $UO_2$ calls for advanced theoretical and computational techniques, e.g., DFT + DMFT, which is widely applied to study the strongly correlated actinide-based materials.[3,15–17] In addition, lots of reported experimental and theoretical results[67–70] provide us with abundant reference. Hence $UO_2$ is a good benchmark system to test our charge self-consistent DFT + DMFT formalism and implementation.

Under the ambient pressure, the stoichiometric $UO_2$ crystallizes in a cubic fluorite ($CaF_2$) structure with the space group $Fm\bar{3}m$. The lattice constant is 5.4682 Å.[71] A $\Gamma$-centered $11 \times 11 \times 11$ $\boldsymbol{k}$-mesh was employed for the integration over the Brillouin zone. All DMFT calculations were carried out by the Rutgres eDMFT impurity solver at temperature of 300 K with $U$ and $J$ parameters of 5.5 eV and 0.5 eV, respectively.

Figure 5 shows the charge self-consistent DFT + DMFT total density of states (DOS) of $UO_2$ and partial DOS (PDOS) of uranium 5f electrons. Our charge self-consistent DFT + DMFT calculation successfully opens an insulating band gap resulting from the strong correlation among 5f electrons. The gap is mainly governed by the energy difference between the upper and lower Hubbard bands of 5f electrons, which is in good agreement with the experimental[70] and theoretical[68,69] results, indicating that $UO_2$ is a Mott insulator. Although the predicted band gap of 2.3 eV shows small quantitative difference from the experimental band gap of 2.1 eV, a better agreement can be achieved by adjusting the $U$ and $J$ parameters. Below $-3.0$ eV, both our charge self-consistent DFT + DMFT result and previous theoretical results of Yin *et al.* and Huang *et al.* predict a strong peak mainly consisting of oxygen 2p electrons. The Zhang–Rice state[68,69] located at around $-2.0 \sim 0.0$ eV and the upper Hubbard band above 2.0 eV obtained by our charge self-consistent DFT + DMFT calculations conform well to experimental[70] and previous theoretical[68,69] results. Nevertheless, the Zhang–Rice state of our result is narrower than experimental[70] and theoretical[68,69] results. This deviation may result from two reasons. The first one is the numerical error introduced by the analytical continuation method and the MEM (maximum entropy method) code. The second one is the error caused by different Brillouin zone sampling, integration, and smearing methods for the calculation of the DOS. In comparison to the one-shot results, the main features of the 5f electrons of one-shot and charge self-consistent calculations are similar. However, the one-shot calculation cannot reproduce the strong peak of oxygen 2p electrons located at around $7.0 \sim -3.0$ eV predicted by previous theoretical calculations. This difference may be arisen from the self-consistence on the charge density, because the self-consistency charge density can also impose influence on the hybridization electrons.

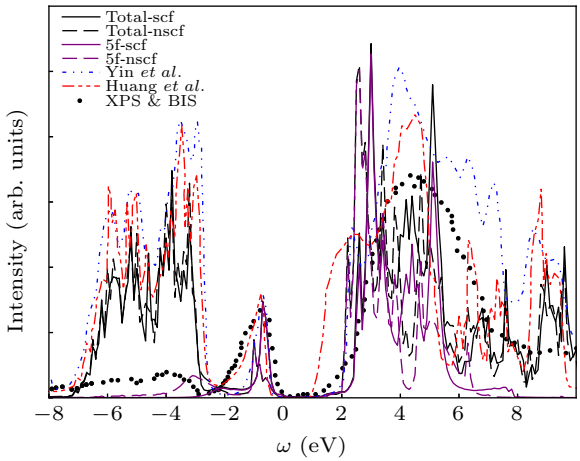



**Fig. 5.** The charge self-consistent DFT + DMFT DOS of $UO_2$ in comparison to previous theoretical and experimental results. The solid black line and purple line are the total DOS and PDOS of 5f electrons of $UO_2$ given by our charge self-consistent DFT + DMFT scheme, while the dashed black line and purple line are the total DOS and PDOS of 5f electrons of $UO_2$ given by our one-shot DFT + DMFT scheme. The theoretical results of Yin *et al.* and Huang *et al.* are taken from Refs. [68,69]. The XPS (x-ray photoemission) and BIS (Bremsstrahlung-isochromat-spectroscop) experiment results are obtained from Ref. [70].

## 5. Summary

We present a charge self-consistent DFT + DMFT formalism within the framework of LCNAO based on our recent one-shot DFT + DMFT work. We implement such formalism by interfacing the NAO-based code FHI-aims, with three CT-HYB impurity solvers, i.e., PACS, iQIST,[44–46] and the Rutgers impurity solver.[30,47] Generally, this formalism and its implementation can play a role of the bridge between the NAO-based DFT codes and impurity solvers. Our formalism and implementation were benchmarked on several prototypical strongly correlated materials belonging to three well-known strongly correlated materials serials, namely, the 3d electron systems $SrVO_3$ and NiO, 4f lanthanides $\alpha$- and $\gamma$-Ce, and 5f actinide $UO_2$. The spectral functions and DOS conform well to previous theoretical and experimental results. In comparison to the previous LCNAO based DFT + DMFT package,[37,72] our implementation can do not only one-shot calculations but also charge self-consistent DFT + DMFT calculations. In addition, our implementation can apply to all strongly correlated systems, e.g., the 5f systems, benefited from the full-potential all-electron technique of FHI-aim.

## Program availability

The source code of our implementation is freely accessible in https://github.com/Qx80610702/DFT_plus_DMFT and also openly available in Science Data Bank at https://doi.org/10.57760/sciencedb.j00113.00123.

## References


[1] Anisimov V V, Zaanen J and Andersen O K 1991 *Phys. Rev. B* **44** 943
[2] Georges A, Kotliar G, Krauth W and Rozenberg M J 1996 *Rev. Mod. Phys.* **68** 13
[3] Kotliar G, Savrasov S Y, Haule K, Oudovenko V S, Parcollet O and Marianetti C A 2006 *Rev. Mod. Phys.* **78** 865
[4] Held K 2007 *Adv. Phys.* **56** 829
[5] Metzner W and Vollhardt D 1989 *Phys. Rev. Lett.* **62** 324
[6] Anisimov V I, Poteryaev A I, Korotin M A, Anokhin A O and Kotliar G 1997 *J. Phys. Condens. Matter* **9** 7359
[7] Lichtenstein A I and Katsnelson M I 1998 *Phys. Rev. B* **57** 6884
[8] Perdew J P and Zunger A 1981 *Phys. Rev. B* **23** 5048
[9] Becke A D 1993 *J. Chem. Phys.* **98** 5648
[10] Heyd J, Scuseria G E and Ernzerhof M 2003 *J. Chem. Phys.* **118** 8207
[11] Li C, Zheng X, Su N Q and Yang W 2018 *Natl. Sci. Rev.* **5** 203
[12] Su N Q, Mahler A and Yang W 2020 *J. Phys. Chem. Lett.* **11** 1528
[13] Su N Q, Li C and Yang W 2018 *Proc. Natl. Acad. Sci. USA* **115** 9678
[14] Anisimov V I, Solovyev I V, Korotin M A, Czyżyk M T and Sawatzky G A 1993 *Phys. Rev. B* **48** 16929
[15] Savrasov S Y, Kotliar G and Abrahams E 2001 *Nature* **410** 793
[16] Dai X, Savrasov S Y, Kotliar G, Migliori A, Ledbetter H and Abrahams E 2003 *Science* **300** 953
[17] Shim J H, Haule K and Kotliar G 2007 *Nature* **446** 513
[18] Shim J H, Haule K and Kotliar G 2007 *Science* **318** 1615
[19] Savrasov S Y and Kotliar G 2004 *Phys. Rev. B* **69** 245101
[20] Hampel A, Beck S and Ederer C 2020 *Phys. Rev. Res.* **2** 033088
[21] Beck S, Hampel A, Parcollet O, Ederer C and Georges A 2022 *J. Phys. Condens. Matter* **34** 235601
[22] Plekhanov E, Hasnip P, Sacksteder V, Probert M, Clark S J, Refson K and Weber C 2018 *Phys. Rev. B* **98** 075129
[23] Marzari N and Vanderbilt D 1997 *Phys. Rev. B* **56** 12847
[24] Marzari N, Mostofi A A, Yates J R, Souza I and Vanderbilt D 2012 *Rev. Mod. Phys.* **84** 1419
[25] Mostofi A A, Yates J R, Lee Y S, Souza I, Vanderbilt D and Marzari N 2008 *Comput. Phys. Commun.* **178** 685
[26] Mostofi A A, Yates J R, Pizzi G, Lee Y S, Souza I, Vanderbilt D and Marzari N 2014 *Comput. Phys. Commun.* **185** 2309
[27] Schüler M, Peil O E, Kraberger G J, *et al.* 2018 *J. Phys. Condens. Matter* **30** 475901
[28] Amadon B 2012 *J. Phys. Condens. Matter* **24** 075604
[29] Gonze X, Jollet F, Abreu Araujo F, Adams D, *et al.* 2016 *Comput. Phys. Commun.* **205** 106
[30] Haule K, Yee C H and Kim K 2010 *Phys. Rev. B* **81** 195107
[31] Bhandary S, Assmann E, Aichhorn M and Held K 2016 *Phys. Rev. B* **94** 155131
[32] Grånäs O, Di Marco I, Thunström P, Nordström L, Eriksson O, Björkman T and Wills J 2012 *Comput. Mater. Sci.* **55** 295
[33] Soler J M, Artacho E, Gale J D, García A, Junquera J, Ordejón P and Sánchez-Portal D 2002 *J. Phys. Condens. Matter* **14** 2745
[34] Delley B 2000 *J. Chem. Phys.* **113** 7756
[35] Blum V, Gehrke R, Hanke F, Havu P, Havu V, Ren X, Reuter K and Scheffler M 2009 *Comput. Phys. Commun.* **180** 2175
[36] Li P, Liu X, Chen M, Lin P, Ren X, Lin L, Yang C and He L 2016 *Comput. Mater. Sci.* **112** 503
[37] Sim J H and Han M J 2019 *Phys. Rev. B* **100** 115151
[38] Qu X, Xu P, Li R, Li G, He L and Ren X 2022 *J. Chem. Theory Comput.* **18** 5589
[39] Pulay P 1980 *Chem. Phys. Lett.* **73** 393
[40] Kresse G and Furthmüller J 1996 *Phys. Rev. B* **54** 11169
[41] Perdew J P, Burke K and Ernzerhof M 1996 *Phys. Rev. Lett.* **77** 3865
[42] Werner P, Comanac A, De' Medici L, Troyer M and Millis A J 2006 *Phys. Rev. Lett.* **97** 076405
[43] Li G 2015 *Phys. Rev. B* **91** 165134
[44] Huang L, Wang Y, Meng Z Y, Du L, Werner P and Dai X 2015 *Comput. Phys. Commun.* **195** 140
[45] Huang L 2017 *Comput. Phys. Commun.* **221**
[46] iQIST
[47] Haule K 2007 *Phys. Rev. B* **75** 155113
[48] CTQMC impurity solver of eDMFT
[49] Monkhorst H J and Pack J D 1976 *Phys. Rev. B* **13** 5188
[50] Lechermann F, Georges A, Poteryaev A, Biermann S, Posternak M, Yamasaki A and Andersen O K 2006 *Phys. Rev. B* **74** 125120
[51] Amadon B, Lechermann F, Georges A, Jollet F, Wehling T O and Lichtenstein A I 2008 *Phys. Rev. B* **77** 205112
[52] Pavarini E, Biermann S, Poteryaev A, Lichtenstein A I, Georges A and Andersen O K 2004 *Phys. Rev. Lett.* **92** 176403
[53] Anisimov V I and Lukoyanov A V 2014 *Acta Crystallogr. Sect. C Struct. Chem.* **70** 137
[54] Anisimov V I, Kondakov D E, Kozhevnikov A V, *et al.* 2005 *Phys. Rev. B* **71** 125119
[55] Nekrasov I A, Held K, Keller G, *et al.* 2006 *Phys. Rev. B* **73** 155112
[56] Nekrasov I A, Keller G, Kondakov D E, Kozhevnikov A V, Pruschke T, Held K, Vollhardt D and Anisimov V I 2005 *Phys. Rev. B* **72** 155106
[57] Sekiyama A, Fujiwara H, Imada S, *et al.* 2004 *Phys. Rev. Lett.* **93** 156402
[58] Ren X, Leonov I, Keller G, Kollar M, Nekrasov I and Vollhardt D 2006 *Phys. Rev. B* **74** 195114
[59] Kuneš J, Anisimov V I, Lukoyanov A V and Vollhardt D 2007 *Phys. Rev. B* **75** 165115
[60] Sawatzky G A and Allen J W 1984 *Phys. Rev. Lett.* **53** 2339
[61] Held K, McMahan A K and Scalettar R T 2001 *Phys. Rev. Lett.* **87** 276404
[62] Bieder J and Amadon B 2014 *Phys. Rev. B* **89** 195132
[63] Amadon B, Biermann S, Georges A and Aryasetiawan F 2006 *Phys. Rev. Lett.* **96** 066402
[64] Grioni M, Weibel P, Malterre D, Baer Y and Duò L 1997 *Phys. Rev. B* **55** 2056
[65] Weschke E, Laubschat C, Simmons T, Domke M, Strebel O and Kaindl G 1991 *Phys. Rev. B* **44** 8304
[66] Wen X D, Martin R L, Henderson T M and Scuseria G E 2013 *Chem. Rev.* **113** 1063
[67] Yin Q and Savrasov S Y 2008 *Phys. Rev. Lett.* **100** 225504
[68] Yin Q, Kutepov A, Haule K, Kotliar G, Savrasov S Y and Pickett W E 2011 *Phys. Rev. B* **84** 195111
[69] Huang L, Wang Y and Werner P 2017 *Europhys. Lett.* **119** 57007
[70] Baer Y and Schoenes J 1980 *Solid State Commun.* **33** 885
[71] Barrett S A, Jacobson A J, Tofield B C and Fender B E F 1982 *Acta Crystallogr. Sect. B Struct. Crystallogr. Cryst. Chem.* **38** 2775
[72] https://kaist-elst.github.io/DMFTpack/